Catalysis Science & Technology

Accepted Manuscript

This article can be cited before page numbers have been issued, to do this please use: J. J. Villora-Pico, I. Campello-Gómez, J. C. Serrano-Ruiz, M. M. Pastor-Blas, A. Sepulveda-Escribano and E. V. Ramos Fernandez, *Catal. Sci. Technol.*, 2021, DOI: 10.1039/D1CY00140J.

ROYAL SOCIETY OF CHEMISTRY

rsc.li/catalysis

View Article Online
DOI: 10.1039/D1CY00140J

ARTICLE

Hydrogenation of 4-nitrochlorobenzene catalysed by cobalt nanoparticles supported on nitrogen-doped activated carbon

Received 00th January 20xx,
Accepted 00th January 20xx

DOI: 10.1039/x0xx00000x

J.J. Villora-Picó[a], I. Campello-Gómez[a], J.C. Serrano-Ruiz[b], M.M. Pastor-Blas[a], A. Sepúlveda-Escribano[a], E.V. Ramos-Fernández*[a]

The hydrogenation of nitroarenes to produce the corresponding amines using dihydrogen as reducing agent has an important industrial role, since it allows to obtain important added-value products. This reaction needs the help of a catalyst to proceed. Many catalysts have been already tested and studied. Most of them are based on noble metals supported on metal oxides. These catalysts perform well, but they are expensive and thus, alternative systems are needed. In this context, cobalt-based catalysts have emerged as adequate alternatives, despite cobalt nanoparticles *per se* are not very active for this reaction. A way to improve the catalytic activity of cobalt nanoparticles is by supporting them on a support with functional groups that are able to change their intrinsic properties and to enhance their catalytic properties. In this sense, N-containing carbons are promising candidates to be used as support, since nitrogen functionalities may modify the catalytic properties of cobalt. In this work, cobalt nanoparticles supported on N-doped activated carbons have been prepared and studied as catalysts for the hydrogenation of 1-chloro-4-nitrobencene to the corresponding chloro-aniline. It is demonstrated that the catalytic activity is enhanced by the presence of nitrogen species in the support. When the temperature of the catalyst activation treatment (reduction under flowing hydrogen) is increased, the catalytic activity increases drastically in the presence of nitrogen functionalities on the support. The catalysts have been characterised by transmission electron microscopy (TEM), temperature-programmed reduction (TPR), X-ray diffraction, X-ray photoelectron spectroscopi (XPS) and N_2 adsorption at 77 K. It has been found that the enhanced catalytic activity was due to two different factors, namely the interaction of the cobalt particles with the nitrogen functional groups (forming Co_4N), and the development of mesopores in the support during the activation process that increases the accessibility of reactants to the active sites.

Introduction

Arenes are a type of organic molecules which encompasses a huge variety of compounds. There is a myriad of applications of these molecules, from the synthesis of drugs and medicaments[1], their use as solvents [2], fine chemistry products in perfumery and for polymer synthesis [3]. Nitroarenes are one special type of arenes that contain a nitro group attached to the benzene ring, arising different properties and enabling different features. Besides, nitroarenes are often used as explosives [4], they are important intermediates in different organic synthesis [5], and the most common use relies on their application as raw materials for the synthesis of aniline [6]. Aniline is an organic solvent largely involved in multitude of processes[7], as well as the precursor for the synthesis of different polymers, fertilizers and other products [8].

The hydrogenation of nitroarenes to obtain different anilines is a highly interesting process for industry. Nitroarene reduction can be achieved by several ways, such as using stoichiometric reducing agents (Zn, Al, Sn, etc.) [6,9,10], electrochemically or by catalytic hydrogenation using sodium borohydride or dihydrogen as reducing agent. The latest one is the preferred method for economic and environmental reasons. When catalytic hydrogenation methods are used, the catalysts are obviously a key factor to effectively produce the anilines, and this is the case when both sodium borohydride or dihydrogen are used as reductants. Catalysts based on noble metals such as Pd [11–13], Pt [14–16] or Au [17,18] are the most used ones due to their high effectiveness. In all these cases the active noble metals are scarce and expensive, so a more convenient alternative is strongly needed.

Cobalt is known to be an excellent catalyst for many reactions such as cycloadditions [19], Fischer-Tropsch [20–23], oxidations [24,25] and hydrogenations [26–28], and it may be a cheaper and more available alternative for the substitution of the noble metal-based catalysts that are currently used for the hydrogenation of nitroarenes. Cobalt nanoparticles by themselves are not efficient for nitroarenes reduction, and they need to be promoted by the support or additives to improve their intrinsic properties. One of the cheapest supports that might be used in catalytic applications are activated carbons. They are also easily tailored and chemically stable during hydrogenation reactions. However, activated carbons without any functional groups are rather inert

[a] Laboratorio de Materiales Avanzados, Departamento de Química Inorgánica – Instituto Universitario de Materiales de Alicante, Universidad de Alicante, Apartado 99, Alicante, E-03080, Spain
[b] Materials and Sustainability Group, Department of Engineering, Universidad Loyola Andalucía, Avda. de las Universidades s/n, 41704 Dos Hermanas, Seville, Spain

† Footnotes relating to the title and/or authors should appear here.
Electronic Supplementary Information (ESI) available: [The supporting information contains additional data suchs as: Elligam diagram and X-ray photoelectron spectrocopy]. See DOI: 10.1039/x0xx00000x

View Article Online
DOI: 10.1039/D1CY00140J

and, in principle, they do not have the capability to promote the metallic active phase[29].

The introduction of heteroatoms in the activated carbon matrix constitutes a route that allows to change the electronic properties of the support and, consequently, opens the possibility to a promotion effect on the supported metal particles. It has been demonstrated that the presence of nitrogen functionalities in activated carbons can help in the hydrogen dissociation step when metal nanoparticles are supported on them. [27,30–32].

Beller's group has developed several strategies to prepare cobalt nanoparticles supported on nitrogen-containing carbons. First, they prepared the catalysts by pyrolyzing non-volatile Co-amine complexes at high temperature [33]. Later on, they also prepared a new generation of catalysts by controlled decomposition of metal organic frameworks. In this way they used a cobalt-based MOF constructed with 1,4-diazabicyclo[2.2.2]octane (DABCO) and terephthalic acid (TPA) as linkers [34]. Using both approaches they found that the presence of nitrogen functionalities was the key factor for the enhanced activity and selectivity. The Gascon's group also used Co nanoparticles supported on nitrogen-containing carbon prepared by decomposition of ZIF-67 [31]. They found that the interaction of the carbon support with the cobalt nanoparticles was very important to determine the catalytic performance. Indeed, it must be taken into account that the cobalt nanoparticles they prepared were embedded into the carbon matrix. In this sense, sintering of the metal particles was prevented, and some additional stability was provided. Both groups prepared these new catalysts using expensive precursors, metal complexes and MOFs, which means that they would be as expensive as those prepared with noble metals, whose precursors are also costly. Moreover, the synthesis protocol for those precursors requires the use of organic solvents, which makes these methods far from being considered environmentally friendly. Besides these practical issues, it is also important to remark that the comparison of the prepared catalysts against their analogous without nitrogen functionalities is not possible.

In this paper we have prepared Co nanoparticles supported on both nitrogen-free and nitrogen-doped activated carbons. The undoped activated carbon was a commercial one (RGC30) [35–37]. Unlike previously reported preparation methods using expensive precursors, MOFs and organic solvents, we herein propose a simpler and cheaper methodology based on melamine as the nitrogen precursor, which is simply impregnated, polymerized and pyrolized on the RGC30 commercial activated carbon[38,39]. Then, the cobalt catalysts were prepared by a well-stablished impregnation method using water as a solvent and cobalt nitrate as the metal precursor.

Experimental

Synthesis of the carbon supports and the catalysts

The nitrogen-containing support was prepared by mechanically mixing melamine and a commercial activated carbon (RGC30), followed by a heat treatment under nitrogen atmosphere. Thus, a mixture of RGC30/melamine 1:4 ratio in weight was physically mixed in a mortar, and then treated at 800 ºC for 1 h under nitrogen flow (100 mL/min) in an horizontal tubular furnace, with a heating rate of 3 ºC/min.

Both carbon supports, N-free and N-doped, were impregnated with the cobalt precursor by the wet impregnation method. 10 mL of aqueous solution of cobalt nitrate ($Co(NO_3)_2 \cdot 6H_2O$) were added to 1 g of support in order to obtain 5 wt.% mass of cobalt in the catalyst. The mixture was then stirred in a rotary evaporator for 24 h, and then vacuum was applied at 70 ºC until complete evaporation of water. After this step, the carbons impregnated with the cobalt precursor were submitted to a heat treatment at 210 °C for 3 h to decompose the cobalt precursor. The obtained materials were named as AC (cobalt supported on non-doped activated carbon) and NAC (cobalt supported on N-doped activated carbon).

Characterization

Temperature-programmed reduction (TPR) measurements were carried out in a U-shaped quartz cell using a 5% H_2/He gas flow of 50 mL/min, with a heating rate of 5 °C/min until 1000 ºC. The different gases released were monitored by on-line mass spectrometry (Omnistar TM Balzers).

The XR diffractograms of the prepared materials were collected using a Bruker equipment, model D8-Advance, provided with a copper anode and a Göebel mirror to avoid the need of removing the Cu K_β radiation with a Ni filter. Therefore, the Cu K_α radiation was used. The samples were scanned with a 2theta angle between 2.5 º and 80 º with an angular speed of 1º/min, a step of 0.05 s and a preset time of 3 s.

TEM images were obtained with a JEM 2010 microscope. The acquisition of the images was made by means of a digital camera GATAN ORIUS SC600 mounted on-axis, integrated with the program GATAN Digital Micrograph 1.80.70 for GMS 1.8.0.

RAMAN spectroscopy was carried out in a Raman Jasco NRS-5100 equipment using a 532 nm laser and a 600 lines/mm slit between 0-4000 cm^{-1}.

X-Ray photoelectron spectroscopy (XPS) was performed with a K-ALPHA spectrometer (Thermo Scientific). All spectra were collected using Al-Kα radiation (1486.6 eV), monochromatized by a twin crystal monochromator, yielding a focused X-ray spot with a diameter of 400 nm, at 3 mA × 12 kV. The alpha hemispherical analyzer was operated at the constant energy mode with survey scan pass energies of 200 eV to measure the whole energy band and 50 eV in a narrow scan to selectively measure the particular elements. Charge compensation was achieved with the system flood gun that provides low energy electrons and low energy argon ions from a single source. The powder samples were pressed and mounted on the sample holder and placed in the vacuum chamber. Before recording the spectrum, the samples were maintained in the analysis chamber until a residual pressure of ca. 5×10^{-7} N/m^2 was reached. The quantitative analysis was estimated by calculating the integral of each peak, after subtracting the S-shaped background, and by

View Article Online
DOI: 10.1039/D1CY00140J

fitting the experimental curve to a combination of Lorentzian (30%) and Gaussian (70%) lines.

Catalytic tests

Before reaction, all catalysts were reduced under a H_2 flow at different temperatures. The catalysts prepared with the parent N-free carbon support were named as "AC number" (where number is the temperature of reduction in ºC); i.e., a sample reduced at 750 ºC is named as AC 750. The catalysts prepared with the N-doped carbon support were labelled as "NAC number", following the same way that for the AC samples.

The catalytic experiments were performed in a 300 mL batch-type reactor (Biometa), equipped with a system that allows liquid sampling. The experiments were carried out with an initial hydrogen pressure of 50 bar at 100 ºC. The previously reduced catalyst (100 mg) and 1.56 g of 4-nitrochlorobenzene (NCB) were added to 100 mL of ethanol, which is used as solvent. In all cases 320 µL of octane was added as internal standard. The system was heated under minimal stirring rate (10 rpm) allowing proper heat transfer but hindering mass transfer to avoid reaction. Zero time was fixed once reaching 100 ºC, and in this moment the stirring rate was increased to 300 rpm. Liquid samples were analyzed with a gas chromatograph equipped with a mass spectrometer and a capillary Carbowax column, using helium as carrier gas.

Results and discussion

Support Preparation

Melamine (2,4,6-triamino-1,3,5-triazina) is a cheap organic compound widely used in the polymer industry to prepare different types of resins. The melting point of melamine is 350 ºC, and it has been reported that above this temperature the melamine molecules self-condensate to generate the so-called graphite carbon nitride g-C_3N_4, that has unique properties in catalysis[40] and photocatalysis[31]. One of the main limitations of these type of materials is their modest surface area that range from 20 to 200 m^2/g [41].

In this paper, a commercial activated carbon has been mechanically mixed with melamine. At a temperature above its melting point, the liquid melamine was adsorbed on the activated carbon by capillarity and, when the temperature was increased, the melamine condensate inside the porosity of the activated carbon. In this way, a g-C_3N_4-like coating has been prepared on the surface of the activated carbon. The resulting material is expected to have a high surface area, resembling that of the parent activated carbon. Figure 1a shows the N_2 adsorption isotherms at 77 -196 ºC of the commercial activated carbon RGC30 and its analogous impregnated with melamine and heat treated. As it can be seen, the adsorption capacity of the RGC30 parent carbon decreases when it is impregnated with melamine. Thus, the surface area of RGC30 is 1400 m^2/g, and that of the same carbon impregnated with melamine is 1100 m^2/g. The shape of the isotherms does not change significantly, this indicating that melamine is homogeneously impregnated and only the narrowest pores are blocked by melamine incorporation. However, it is important to remark that the mesopore volume is high for both samples, which is highly recommended for catalytic applications in the liquid phase.

Catalysts characterization

Both supports, the parent activated carbon and the activated carbon modified with melamine, were impregnated with cobalt nitrate as it has been explained in the experimental section.

Nitrogen adsorption isotherms

The prepared catalysts were first characterized by N_2 adsorption isotherm at -196 ºC. The adsorption isotherms are shown in Figure 1. As it can be seen, the impregnation with cobalt does not produce any significant loss of apparent surface area, which is an indication that the cobalt particles are well dispersed and they do not block pores.

Temperature programmed reduction

As it is shown below, the temperature of reduction is a key factor that controls the catalytic performance of the catalysts tested in this work. In order to study their reducibility, temperature-programmed reduction experiments under H_2 were conducted with both samples. Figure 2 shows the corresponding TPR profiles. Three well differentiated reduction peaks can be seen in the TPR profile of sample AC, which are associated with water evolution. This implies that the hydrogen is consumed in a reduction process and it is oxidized to water [42]. The peaks found at 260, 400 ºC are assigned to the reduction of Co(III) to Co(II), followed by the reduction of Co(II) to Co(0). The peak centered at 550 ºC is associated to carbon methanation catalyzed by metallic cobalt, as it can be evidenced by the evolution of methane during this experiment (See Figure 3).

The TPR profile of the NAC sample (Figure 2) shows two peaks; the first peak at lower temperature appears at 200 ºC, instead of 260 ºC as it is the case for AC, and corresponds to the reduction of oxidic cobalt species to metallic cobalt. The shifting of the

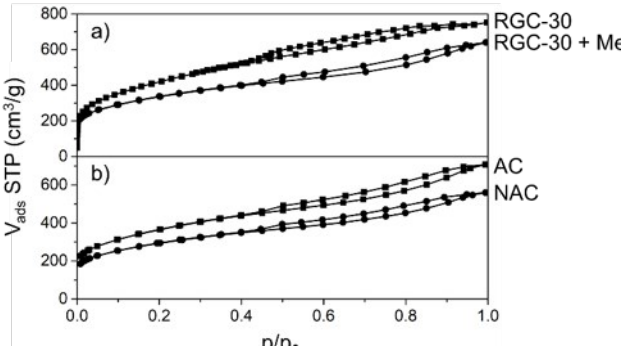

Figure 1. a) N_2 adsorption isotherms at 77 K of the commercial activated carbon (RGC30) and the melamine-modified activated carbon (RGC30+Mel). b) N_2 adsorption isotherms at 77 K of both supports impregnated with cobalt nitrate and calcined (AC and NAC).

View Article Online
DOI: 10.1039/D1CY00140J

reduction temperature from to 260 to 200 ºC is ascribed to the higher interaction of the cobalt species with the support, that can be due to the presence of nitrogen functional groups that not only favor the anchoring of the cobalt species to the support, but also enhance their reducibility. The broad peak at higher temperature is centered at 515 ºC in NAC, whereas it was observed at 550 ºC in AC. This peak it associated to the methanation of the carbon support catalyzed by cobalt particles. The lower temperature of these peaks in NAC suggest that the presence of nitrogen groups enhances both, the reduction of the cobalt oxide particles and also the methanation of the carbon support.

In order to further clarify the results of the TPR experiments, the evolution of other gases has also been checked. Figure 3 shows the evolution profiles of CO, CO_2 and H_2O during the TPR experiments with AC and NAC samples. For NAC, since there is no H_2O, CO and CO_2 associated to the second peak have been assigned to methane evolution, which is further confirmed by following the m/z = 16 and 15 signals. This methane evolution is due to the carbon methanation process catalyzed by the metallic cobalt particles. On the other hand, the first peak which is associated to H_2O, CO and CO_2 evolution, is ascribed to the reduction of cobalt oxide particles. The TPR results of the AC samples clearly differ from those from the NAC sample at 550 ºC.

The released gases are those expected when the Ellingham diagram is considered (Figure S1). At temperatures higher than 200 ºC, the reduction of CoO with carbon to yield CO_2 becomes spontaneous, and reaction takes place for both samples; it is more intense for the NAC sample, what may be due to the strong interaction between cobalt particles and the carbon. On the other hand, the reduction of CoO with C to yield CO is spontaneous at temperatures higher than 500 ºC, and in both samples there is a peak of CO evolution centered between 500-600 ºC, which also takes place at lower temperature in the case of NAC samples.

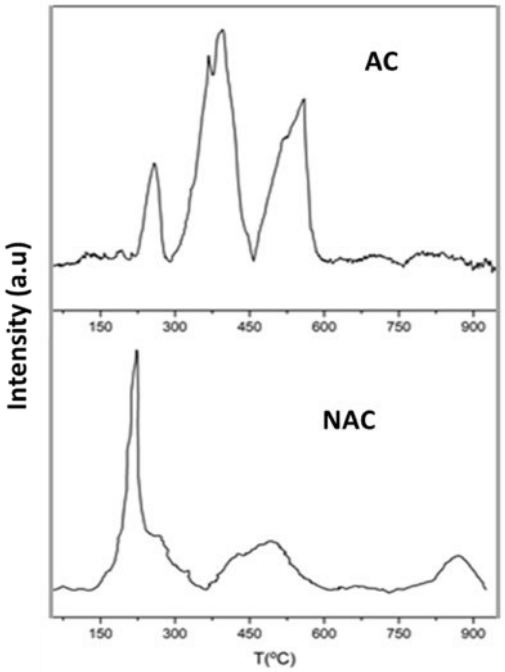

Figure 2. Temperature-programmed reduction profiles (hydrogen consumption) of AC and NAC samples.

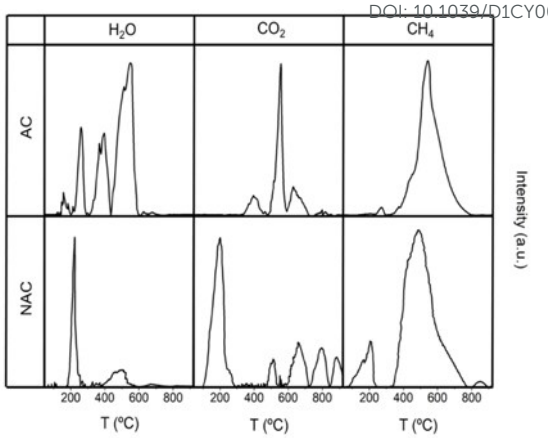

Figure 3. Evolution of different gases during temperature programmed reaction

From the above results it is possible to propose a series of reactions taking place during the reduction process. First, the reactions corresponding to the reduction of the metal oxides with hydrogen (1 and 2) that imply water formation and hydrogen consumption; then, reactions 3 and 4 that correspond to those showed in the Ellingham diagram (See Figure S1) where the carbon support is able to reduce the cobalt oxides forming CO_2 and CO, respectively. Lastly, the methanation of carbon catalyzed by metallic cobalt particles (5) takes place around 515-550 ºC, with H_2 consumption and evolution of CH_4. These reactions fit well with the gases released during the TPR experiment, as well as with the expected temperatures extracted from the Ellingham diagram and the literature [42,43].

$$\mathbf{1.}\ Co_2O_3 + H_2 \rightarrow 2CoO + H_2O$$
$$\mathbf{2.}\ CoO + H_2 \rightarrow Co + H_2O$$
$$\mathbf{3.}\ 2CoO + C \rightarrow 2Co + CO_2$$
$$\mathbf{4.}\ CoO + C \rightarrow Co + CO$$
$$\mathbf{5.}\ C + 2H_2 \rightarrow CH_4$$

Regarding the NAC samples, reactions 1-3 take place at the same temperature (200 ºC), with evolution of water and CO_2 and consumption of H_2. This evidences the strong interactions between the N functionalities and the cobalt particles, causing that all the possible reduction reactions occur at the same temperature. The CO signal might also be detected due to the presence of CO_2, whose presence has an associated CO signal within the detector. Production of CO_2 through reaction 3, by reduction of cobalt oxide by the carbon support, is less favored for the AC catalyst. In fact, CO_2 evolution is mainly observed at 550 ºC for this sample, whereas it is produced at only 200 ºC for the NAC catalyst. Similarly, reaction 4 takes place at 600 ºC. These findings suggest the existence of a higher kinetic barrier for the reduction reaction in the presence of the AC catalyst, since all the reactions take place at higher temperatures than in the presence of the NAC catalyst.

X-ray diffraction

View Article Online
DOI: 10.1039/D1CY00140J

AC samples

XRD patterns of the catalysts were collected after the reduction treatment at different temperatures, and they are reported in Figure 4. As it can be seen, samples reduced at 600 ºC do not show any peaks, which indicates the good dispersion of the cobalt nanoparticles that are too small to be discerned by XRD. When the reduction temperature is increased to 750 ºC a peak at 37.5 shows up. These peak perfectly matches with the diffraction peak corresponding to the (110) plane of Co_2C, indicating that the reduction treatment at high temperature produces preferentially oriented 2D Co_2C (JCPDS 1-072-1369). The carburization step, which has been extensively studied in literature, starts with the reduction of the cobalt species to metallic cobalt; then, the carbon atoms diffuse into the cobalt lattice forming Co_2C [44,45]. The fact that the diffraction peaks of metallic cobalt are not detected means that cobalt nanoparticles are too small to be detected or they have an amorphous nature. The carbide formed through diffusion of carbon species into the cobalt particles is highly oriented, and its enhanced crystallinity allows it to be detected by XRD. Sample AC 900 shows two peaks, at 37.5º (2D Co_2C) and at 43.7º. This latter is ascribed to the diffraction at the (111) plane of metallic cobalt (body centered cubic) (JCPDS 98-005-3805). The presence of both peaks indicates that the increased temperature produces larger cobalt particles that can be detected by XRD. However, it is important to remark the higher intensity of the peak ascribed to Co_2C compared to that of the metallic cobalt. These results are in line with those obtained by XPS (see below).

NAC samples

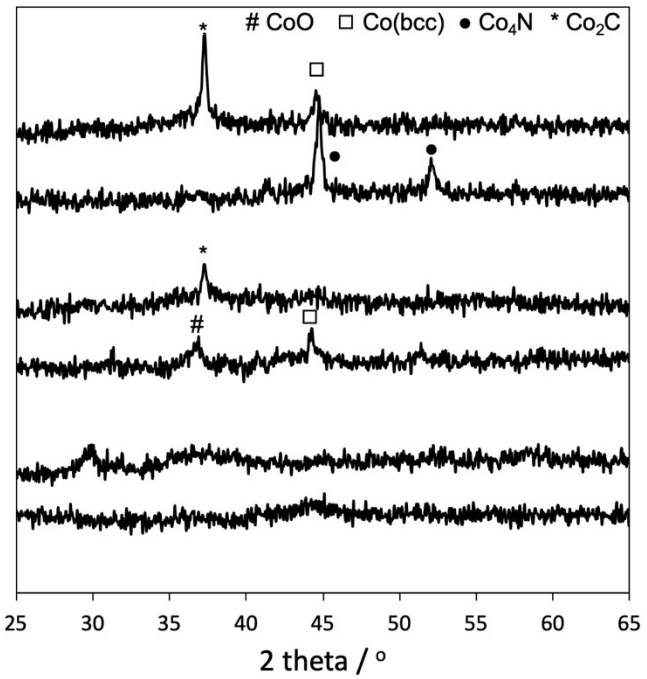

Figure 4. XRD pattern of the AC and NAC samples reduced at different

The cobalt species that are generated upon reduction in the nitrogen-containing catalysts (NAC) are different from those produced in the AC samples. The XRD pattern of the sample reduced at 600 ºC (NAC600) does not present any discernible peaks, indicating the amorphous nature of the species formed. XRD pattern of sample NAC750 shows three peaks centred at 36.9, 42.1 and 51.8º. The first one can be ascribed to oriented 2D Co_2C (JCPDS 1-072-1369). The second and the third ones are ascribed to metallic cobalt. These results, together with those from the AC samples and the TPR profiles, indicate that during the reduction treatment the cobalt species are reduced at temperatures lower than 600 ºC, but the formed particles are not large enough as to be detected by XRD. However, the carburization process begins just when cobalt is reduced, and the cobalt carbide phase starts to growth. The cobalt carbide nanocrystals and the cobalt nanoparticles (temperature of reduction 750 ºC) are more prominent in the NAC sample, indicating that nitrogen functional groups push the reduction and the growth of the cobalt carbide and cobalt nanoparticles.

When the reduction temperature is increased to 900 ºC two peaks show up. Although the one centred at 44.8º could in a first sight be ascribed to metallic cobalt, it is however shifted up 1.5 theta respective to the reported values for the (111) plane of the body centred cubic metallic cobalt. This may be an indication of the formation of cobalt nitride (Co_4N), since nitrogen atoms can occupy the octahedral sites of the cobalt *bcc* structure whether totally or partially, producing a deformation of the structure. The shifting of this peak due to Co_4N formation has been deeply demonstrated in the literature[46–49]. The same situation has also found for the peak at 52.2 ºC. It can then be concluded that the reduction treatment at high temperature (900 ºC) produces differentiated species in AC and NAC, which will probably affect their catalytic properties.

X-ray photoelectron spectroscopy (XPS)

TPR experiments showed that the temperature at which the catalysts are reduced reaction might be a key factor determining the properties of the catalysts. XPS has been used to evaluate the surface chemical composition of the catalysts after reduction under hydrogen at different temperatures.

The XPS spectra of the Co 2p level is shown in Figure 5. The Co 2p level spectra are difficult to analyze, since the signals of different Co species are overlapping in a very narrow range of binding energies. In the case of our samples it becomes especially difficult, since the intensity of the signals decreases when the temperature of reduction increases. This decrease in intensity is related to the loss of cobalt surface species with the reduction treatment. It might be ascribed to both the sintering of cobalt particles with the increasing reduction temperature and/or the coverage of the cobalt particles with carbon. Regarding the oxidation state of the cobalt, it can be seen that AC and NAC samples show different spectra, indicating that the presence of nitrogen functional groups also affects the electronic properties of the cobalt species. Thus, it is important to remark that AC samples show a peak centred at 778 eV that is ascribed to reduced cobalt. This peak is especially prominent in the sample

View Article Online
DOI: 10.1039/D1CY00140J

AC600 and is less pronounced for samples AC750 and AC900, what may be due to the decrease in the amount of surface cobalt species. The more pronounced peak is the one centred at 781 eV, which is linked to a satellite peak centred at 786 eV; these two peaks are ascribed to electron deficient cobalt species that may be formed by surface oxidation after the reduction treatment. The fact that even exposing the sample to air the catalyst is nor fully oxidized is due to the presence of cobalt carbide species.

The NAC samples show a different behaviour. The peak centred at 778 eV is not shown, and only the peaks ascribed to electron deficient cobalt species are present. The absence of reduced cobalt particles must be ascribed to the formation of different cobalt species with respect to AC. It has been published that the interaction of nitrogen species with cobalt produces an electron transfer from cobalt to nitrogen which is specially accentuated when cobalt nitride is formed[49]. This further supports the findings obtained by TPR and XRD analysis.

Figure S2 shows N 1s XPS spectra of N-containing catalysts reduced at different temperatures. The N-doping results effective and doping values of 7 at.% of N in the non-reduced catalyst are achieved. This amount of nitrogen decreases with increasing the reduction temperature, up to 0.7 at.% at 900ºC, what can be explained by the decomposition of the nitrogen functionalities producing N_2 and NH_3. Two types of N groups are present in all samples, those associated with pyridinic-type N at 398.3 eV, and the corresponding pyrrolic N groups at 400.1-400.7 eV. The decrease in nitrogen content could be due to the thermal decomposition of these functionalities. The main difference between the NAC samples is in the kind of groups that are loss during the reduction treatment. Thus, the pyrrolic/pyridinic ratio increases with the reduction temperature, indicating that pyrrolic nitrogen, more electron-rich species, is the most thermally stable and remains in higher amount after reduction at higher temperature.

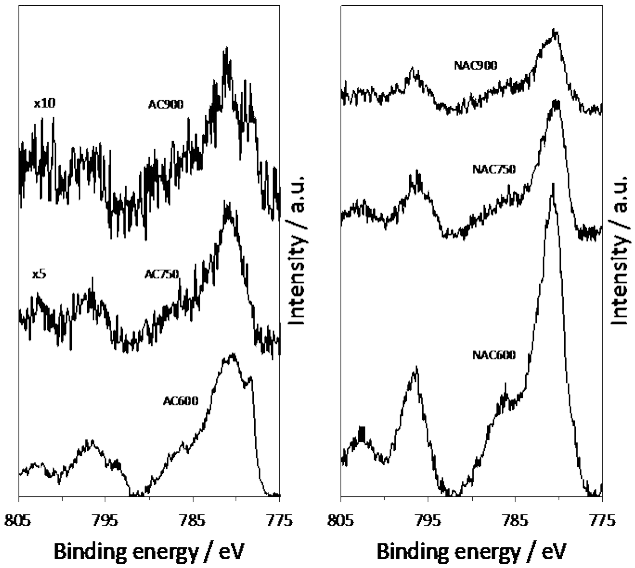

Figure 5. Co 2p core level spectra of all sample after reduction treatment

Raman spectroscopy

Raman spectroscopy provides useful information on the carbon microstructure. It is well known that natural diamond shows a single Raman peak at 1332 cm^{-1}, whereas crystalline graphite shows a Raman peak (referred as the G-peak) at around 1580 cm^{-1} which is ascribed to E_{2g} symmetry of bond-stretching vibrations of sp^2 carbon sites. Amorphous carbon has an additional peak (labelled as the D-peak) at around 1355 cm^{-1} due to the A_{1g} breathing vibrations of the sixfold carbon rings. The D vibration mode is forbidden in an ideal graphite structure, but it appears when disorder increases. Figure 6 show the Raman spectra of the AC600 and the AC900 samples. As it can be seen, both samples show a D-peak which is more developed than the G-peak. If the G and D peaks are deconvoluted and integrated (not shown) the ratio (I_D/I_G) can be calculated, giving a quantitative estimation of the degree of order of the carbon matrix. The value of the I_D/I_G ratio for sample AC600 is 2.9, and it is 2.7 for the sample AC900. These values are high in comparison with other types of carbon materials, as graphite[50] or carbon nanotubes, pointing to the high disorder of the activated carbon, as expected. The sample reduced at high temperature (AC900) has a lower value, indicating that the reduction treatment produces a partial ordering of the carbon structure, as it is also expected. Similar spectra are obtained for the N-doped catalysts, NAC600 and NAC900.

It is interesting to point out that the samples reduced at 900 ºC, either AC900 or NAC900, show a small band at 1200 cm^{-1}. This peak is assigned to aliphatic moieties connected to graphitic basic structural units, as it has been demonstrated by Bokobza et al.[50] This reveals that aliphatic moieties are formed during the reduction treatment at high temperature, and these functional groups are the intermediates in the gasification processes taking place upon reduction.

It is very difficult to discern signals corresponding to Co_2C, since the stretching modes overlap with the carbon signals; furthermore, the amount of Co_2C is very small in comparison with the carbon content.

Textural characterization.

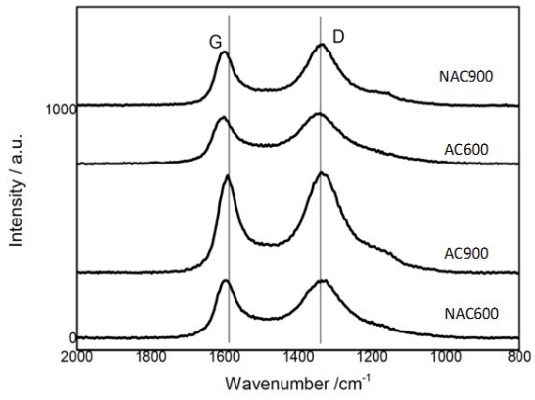

Figure 6. Raman spectra of the AC and NAC samples reduced at different

View Article Online
DOI: 10.1039/D1CY00140J

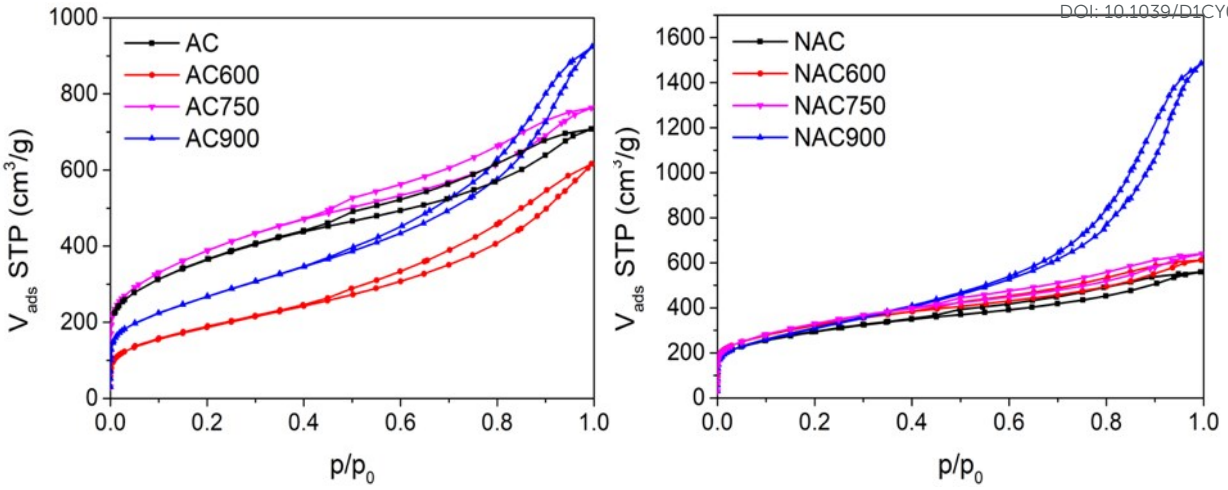

Figure 7. Nitrogen adsorption isotherms at -196 ºC for catalysts reduced at different temperatures

AC samples

Figure 7 shows the N_2 adsorption isotherms at -196 ºC for the AC catalysts after the different reduction treatments. The corresponding textural parameters are reported in Table 1. The reduction treatment at 600 ºC produces a drastic decrease of the surface area as compared with the non-reduced catalyst (AC). This results can be ascribed to the partial obstruction of micropores due to the migration of cobalt particles to the more internal pores[24,32,37,51–53]. When the temperature of reduction was increased to 750 ºC the N_2 uptake increased with respect to AC600 and AC, this indicating that new microporosity is generated upon the reduction process. This microporosity comes from the reaction of the carbon support with hydrogen to yield methane (methanation). The modification of the textural properties is especially remarkable for the sample reduced at 900 ºC. At this high temperature microporosity is decreased whereas mesopores are formed, as can be concluded for the large increase of N_2 uptake at high P/P_o and the decrease at low relative pressure, the change in the shape of the upper part of the isotherm at relative pressures higher than 0.5, and the different hysteresis cycle.

NAC samples

The evolution of the textural properties of N-doped catalysts (NAC) with the reduction temperature is completely different from those of the AC samples (Figure 7). Far from the surface area decrease experienced by AC samples with the increased reduction temperature, NAC samples show a slight increase in surface area at 600 ºC and 750 ºC. This is an indication of the cobalt species being strongly attached to the support. This prevents their migration and the consequent blocking of the narrowest porosity. This strong attachment can be assigned to the presence of the nitrogen groups at the surface of the support. It also indicates that upon reduction at 600 and 750 ºC some methanation of the support occurs. When the temperature of reduction is increased to 900 ºC the shape of the N_2 adsorption isotherm changes. The microporosity (adsorption at low relative pressure) is very similar to that in samples NAC600 and NAC750, however the mesoporisty dramatically increases (see Table 1). This increase in mesoporosity in not followed by a decrease of microporosity as it was observed in AC samples, which indicates that the methanation process follows a different path that can be related to the presence of N groups in the NAC samples.

Transmission electron microscopy (TEM)

Figure 8 shows the TEM images for the catalysts after being reduced at 900 ºC. For both catalysts the mean Co particle size is around 8 nm, with no differences between the N-free and the N-doped catalysts. Interestingly, it can be seen that the cobalt nanoparticles are covered by a carbon shell of 1-2 layers in both the AC900 and NAC900 samples. If we bear in mind that the XRD analysis of the AC900 sample showed a unique peak of the Co_2C crystalline phase, this image proofs that the cobalt particles are surrounded by 2D cobalt carbide. So, it can be concluded that the AC900 catalyst is composed by core-shell particles where the core is metallic cobalt and the shell is 2D highly oriented cobalt carbide. Cobalt particles in the NAC900 sample also show a core-shell structure. However, in this case the shell might have a more amorphous nature, as an ordering cannot be discerned. The shell is probably composed of amorphous carbon, while the core is cobalt nitride (Co_4N), as assessed by XRD.

View Article Online
DOI: 10.1039/D1CY00140J

ARTICLE

Table 1. Textural parameters of the prepared catalysts. V_T: Total pore volume; V_{MESO}: Mesopore volume; V_O: Micropore volume; Sa: Apparent surface area.

SAMPLE	Sa (m^2/g)	V_T (mL/g)	V_{MESO} (mL/g)	V_0 (mL/g)
AC	1270	1.07	0.60	0.47
AC R600	650	0.84	0.62	0.22
AC R750	1370	1.13	0.61	0.52
AC R900	950	1.32	0.95	0.37
NAC R600	1110	0.93	0.44	0.49
NAC R750	1160	0.96	0.53	0.33
NAC R900	1100	2.09	1.58	0.51

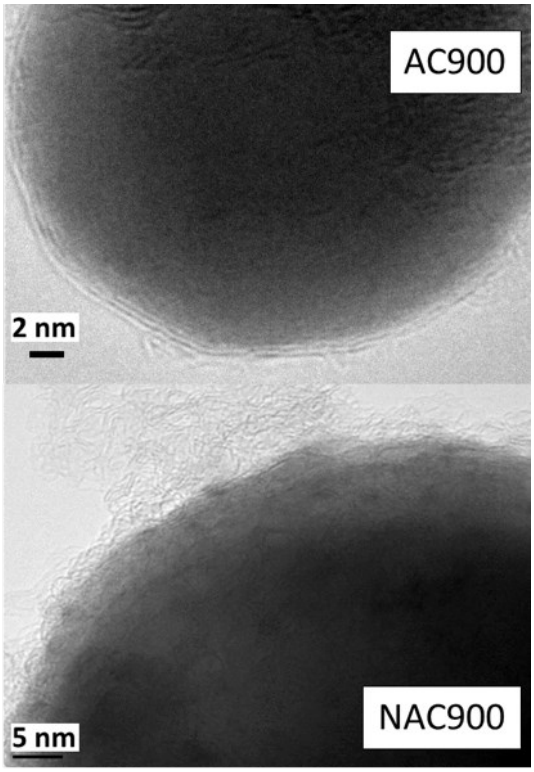

Figure 8. TEM images of NA and NAC catalysts reduced at 900 ºC

Catalytic test

Figure 9 shows the performance of the catalysts reduced at difference temperatures, in terms of conversion degree (%) as a function of reaction time. The RGC-30 parent support catalyzed the reaction even without cobalt, although the conversion is only 24 % after 1200 min (not shown in Figure 9). It is confirmed that the presence of cobalt particles increases the catalytic activity, leading to 37 and 30 % conversion for the AC600 and AC750 samples, respectively, and even higher (58%) for AC900. This enhanced activity can be attributed to two factors; firstly, the mesoporosity is larger in AC900, what facilitates the accessibility of the reactant to the metal particles and, secondly, cobalt is partially reduced (as assessed by XRD analysis). It is known that reduced cobalt catalyses the reaction more effectively that its oxidic forms[26,28,30,54]. It is important to remark that for all measured samples the selectivity was 100% towards the aniline.

The NAC samples show better catalytic activity than the AC samples, and it increases when the reduction temperature

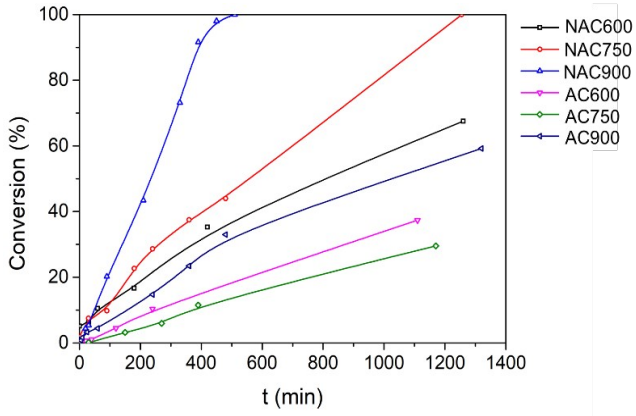

Figure 9. Results of the catalytic test.

increases. This enhanced catalytic activity is ascribed to the presence of the nitrogen functionalities. The nitrogen groups favour two modifications in the structure of the catalyst. The cobalt particles are mainly in the form of Co_4N, as evidenced by XRD analysis. Cobalt nitride is formed by metallic cobalt in a non-dense packing where the nitrogen atoms occupy the octahedral sites. This arrangement facilitates the charge transfer between cobalt and nitrogen atoms. Other important consideration deals with steric effects; the cobalt particles are covered by an amorphous carbon shell that allows the reactant to

View Article Online
DOI: 10.1039/D1CY00140J

reach the cobalt surface. Furthermore, the N_2 adsorption isotherms showed that the porosity of this material is also wider in NAC900, this favouring the accessibility of the reactant to the catalytic active sites. The sum of these factors results in a catalyst with increased activity.

Conclusions

In this contribution we have prepared nitrogen-doped activated carbon, and its role as support for cobalt nanoparticles has been compared with that of the parent activated carbon. We have investigated the effect of the nitrogen groups as well as the reduction treatment in the catalytic reduction of 4-nitrochlorobenzene. We have found that the reduction treatment produces different types of cobalt species. Thus, AC samples reduced at high temperature (900 ºC) are composed of 2D cobalt carbide, whereas its N-doped counterpart is made of Co_4N. This different composition, together with the wider porosity of the N-doped catalyst, can explain the better catalytic behavior of NAC900 and the selective hydrogenation of 4-nitrochlorbenzene to 4-chloroaniline.

Conflicts of interest

"There are no conflicts to declare".

Acknowledgements

Authors acknowledge financial support by MINECO (Spain) through the projects MAT2017-86992-R and MAT2016-80285-P and the European Union for the project "eForFuel", grant agreement 763911. J.C.S.R. would like to thank the Spanish Ministry of Science and Innovation for financial support through the Ramón y Cajal Program, Grant: RYC-2015-19230 J.C.S.R. would also like to thank Junta de Andalucía for financial support through the projects PY18-RE-0012 and IE18_0047_FUNDACIÓN LOYOLA.

Notes and references

1 A. Yousaf, S. A. Hamid, N. M. Bunnori and A. A. Ishola, *Drug Des. Devel. Ther.*, 2015, **9**, 2831–2838.
2 Anon, *ANSI Stand*.
3 C. W. Sathiyajith, R. R. Shaikh, Q. Han, Y. Zhang, K. Meguellati and Y. W. Yang, *Chem. Commun.*, 2017, **53**, 677–696.
4 J. C. Oxley, *Theor. Comput. Chem.*, 2003, **12**, 5–48.
5 E. Łukasik and Z. Wróbel, *Synth.*, 2016, **48**, 263–270.
6 R. S. Downing, P. J. Kunkeler and H. Van Bekkum, *Catal. Today*, 1997, **37**, 121–136.
7 J. F. Hartwig, S. Shekhar, Q. Shen and F. Barrios-Landeros, *Synthesis of Anilines*, 2009.
8 P. L. Milan Králik, Mária Turáková, Ivan Macák, 2014, 723–733.
9 US3975444A, 1991.
10 *Nitro Gr. Org. Synth.*, 2001, 159–181.
11 S. Byun, Y. Song and B. M. Kim, *ACS Appl. Mater. Interfaces*, 2016, **8**, 14637–14647.
12 Y. Lei, Z. Chen, G. Lan, R. Wang and X.-Y. Zhou, *New J. Chem.*, 2020, **44**, 3681–3689.
13 L. Bao, Z. Yu, T. Fei, Z. Yan, J. Li, C. Sun and S. Pang, *Appl. Organomet. Chem.*, , DOI:10.1002/aoc.5607.
14 P. Lara and K. Philippot, *Catal. Sci. Technol.*, 2014, **4**, 2445–2465.
15 D. Gao, S. Li, X. Wang, L. Xi, K. M. Lange, X. Ma, Y. Lv, S. Yang, K. Zhao, H. M. Loussala, A. Duan, X. Zhang and G. Chen, *J. Catal.*, 2019, **370**, 385–403.
16 T.-N. Ye, Z. Xiao, J. Li, Y. Gong, H. Abe, Y. Niwa, M. Sasase, M. Kitano and H. Hosono, *Nat. Commun.*, , DOI:10.1038/s41467-019-14216-9.
17 A. Corma and P. Serna, *Science (80-.).*, 2006, **313**, 332 LP – 334.
18 A. Corma, P. Serna, P. Concepción and J. J. Calvino, *J. Am. Chem. Soc.*, 2008, **130**, 8748–8753.
19 F. Xu, X. J. Si, X. N. Wang, H. D. Kou, D. M. Chen, C. Sen Liu and M. Du, *RSC Adv.*, 2018, **8**, 4895–4899.
20 J. Xie, P. P. Paalanen, T. W. van Deelen, B. M. Weckhuysen, M. J. Louwerse and K. P. de Jong, *Nat. Commun.*, 2019, **10**, 167.
21 A. Dinse, M. Aigner, M. Ulbrich, G. R. Johnson and A. T. Bell, *J. Catal.*, 2012, **288**, 104–114.
22 A. S. M. Ismail, M. Casavola, B. Liu, A. Gloter, T. W. Van Deelen, M. Versluijs, J. D. Meeldijk, O. Stéphan, K. P. De Jong and F. M. F. De Groot, *ACS Catal.*, 2019, **9**, 7998–8011.
23 T. W. van Deelen, H. Yoshida, R. Oord, J. Zečević, B. M. Weckhuysen and K. P. de Jong, *Appl. Catal. A Gen.*, , DOI:10.1016/j.apcata.2020.117441.
24 P. R. Shukla, S. Wang, H. Sun, H. M. Ang and M. Tadé, *Appl. Catal. B Environ.*, 2010, **100**, 529–534.
25 P. Yin, T. Yao, Y. Wu, L. Zheng, Y. Lin, W. Liu, H. Ju, J. Zhu, X. Hong, Z. Deng, G. Zhou, S. Wei and Y. Li, *Angew. Chemie - Int. Ed.*, 2016, **55**, 10800–10805.
26 F. Chen, B. Sahoo, C. Kreyenschulte, H. Lund, M. Zeng, L. He, K. Junge and M. Beller, *Chem. Sci.*, 2017, **8**, 6239–6246.
27 H. Li, C. Cao, J. Liu, Y. Shi, R. Si, L. Gu and W. Song, *Sci. China Mater.*, 2019, **62**, 1306–1314.
28 P. Büschelberger, E. Reyes-Rodriguez, C. Schöttle, J. Treptow, C. Feldmann, A. Jacobi Von Wangelin and R. Wolf, *Catal. Sci. Technol.*, 2018, **8**, 2648–2653.
29 F. Rodríguez-reinoso, *Carbon N. Y.*, 1998, **36**, 159–175.
30 Y. Zhang, P. Cao, H. Y. Zhang, G. Yin and J. Zhao, *Catal. Commun.*, 2019, **129**, 105747.
31 X. Sun, A. I. Olivos-Suarez, L. Oar-Arteta, E. Rozhko, D. Osadchii, A. Bavykina, F. Kapteijn and J. Gascon, *ChemCatChem*, 2017, **9**, 1854–1862.
32 A. L. Yaumi, M. Z. A. Bakar and B. H. Hameed, *Energy*, 2018, **155**, 46–55.
33 F. A. Westerhaus, R. V. Jagadeesh, G. Wienhöfer, M. M. Pohl, J. Radnik, A. E. Surkus, J. Rabeah, K. Junge, H. Junge, M. Nielsen, A. Brückner and M. Beller, *Nat. Chem.*, 2013, **5**, 537–543.

View Article Online
DOI: 10.1039/D1CY00140J

34 R. V Jagadeesh, K. Murugesan, A. S. Alshammari, H. Neumann, M.-M. Pohl, J. Radnik and M. Beller, *Science (80-.).*, 2017, **358**, 326 LP – 332.

35 E. Lam and J. H. T. Luong, *ACS Catal.*, 2014, **4**, 3393–3410.

36 E. Pérez-Mayoral, V. Calvino-Casilda and E. Soriano, *Catal. Sci. Technol.*, 2016, **6**, 1265–1291.

37 A. Gonçalves, J. Silvestre-Albero, E. V. Ramos-Fernández, J. C. Serrano-Ruiz, J. J. M. Órfão, A. Sepúlveda-Escribano and M. F. R. Pereira, *Appl. Catal. B Environ.*, 2012, **113–114**, 308–317.

38 J. Hoekstra, A. M. Beale, F. Soulimani, M. Versluijs-Helder, D. Van De Kleut, J. M. Koelewijn, J. W. Geus and L. W. Jenneskens, *Carbon N. Y.*, 2016, **107**, 248–260.

39 E. Charon, J. N. Rouzaud and J. Aléon, *Carbon N. Y.*, 2014, **66**, 178–190.

40 X. Wang, K. Maeda, A. Thomas, K. Takanabe, G. Xin, J. M. Carlsson, K. Domen and M. Antonietti, *Nat. Mater.*, 2009, **8**, 76–80.

41 D. Feng, Y. Cheng, J. He, L. Zheng, D. Shao, W. Wang, W. Wang, F. Lu, H. Dong, H. Liu, R. Zheng and H. Liu, *Carbon N. Y.*, 2017, **125**, 454–463.

42 M. Cordoba, C. Miranda, C. Lederhos, F. Coloma-Pascual, A. Ardila, G. A. Fuentes, Y. Pouilloux and A. Ramírez, *Catalysts*, 2017, **7**, 1–12.

43 B. Solsona, T. E. Davies, T. Garcia, I. Vázquez, A. Dejoz and S. H. Taylor, *Appl. Catal. B Environ.*, 2008, **84**, 176–184.

44 J. Sheng, L. Wang, L. Deng, M. Zhang, H. He, K. Zeng, F. Tang and Y.-N. Liu, *ACS Appl. Mater. Interfaces*, 2018, **10**, 7191–7200.

45 P. Chen, F. Yang, A. Kostka and W. Xia, *ACS Catal.*, 2014, **4**, 1478–1486.

46 C. Liu, G. Bai, X. Tong, Y. Wang, B. Lv, N. Yang and X.-Y. Guo, *Electrochem. commun.*, 2019, **98**, 87–91.

47 P. Chen, K. Xu, Y. Tong, X. Li, S. Tao, Z. Fang, W. Chu, X. Wu and C. Wu, *Inorg. Chem. Front.*, 2016, **3**, 236–242.

48 X. Zhao, L. Ke, C.-Z. Wang and K.-M. Ho, *Phys. Chem. Chem. Phys.*, 2016, **18**, 31680–31690.

49 L. Wang, W. Zhang, X. Zheng, Y. Chen, W. Wu, J. Qiu, X. Zhao, X. Zhao, Y. Dai and J. Zeng, *Nat. Energy*, 2017, **2**, 869–876.

50 L. Bokobza, J.-L. Bruneel and M. Couzi, *C—Journal Carbon Res.* , 2015, 1.

51 J. Ruiz-Martínez, E. V. V Ramos-Fernández, A. Sepúlveda-Escribano and F. Rodríguez-Reinoso, *Effect of thermal treatments on the surface chemistry of oxidized activated carbons*, 2007, vol. 160.

52 W. Zhao, M. Zhu and B. Dai, *Catal. Commun.*, 2017, **98**, 22–25.

53 J. C. C. Serrano-Ruiz, E. V. V. Ramos-Fernández, J. Silvestre-Albero, A. Sepúlveda-Escribano and F. Rodríguez-Reinoso, *Mater. Res. Bull.*, 2008, **43**, 1850–1857.

54 A. Guerrero-Ruiz, A. Sepúlveda-Escribano and I. Rodríguez-Ramos, *Appl. Catal. A, Gen.*, 1994, **120**, 71–83.